Nanoscale

PAPER

View Article Online
View Journal | View Issue

Cite this: *Nanoscale*, 2024, **16**, 14302

The interplay of chromophore–spacer length in light-induced gold nanocluster self-assembly†

Jose V. Rival, [a] Nonappa [b] and Edakkattuparambil Sidharth Shibu *[a]

The light-induced self-assembly of chromophore-tethered precision nanoclusters (NCs) has recently received significant attention due to their facile control over structure, function, and reversibility under ambient conditions. However, the magnitude of assembly depends on the photoswitching efficiency, chemical structure, and proximity of the chromophore to the NC surface. Herein, using azobenzene alkyl monothiol (AMT)-capped gold NCs with two different spacer lengths (denoted as C_3-NC and C_9-NC), we show that reversible *cis* ↔ *trans* isomerization efficiency can be readily tuned to control the self-assembly kinetics of NCs. Irrespective of the chain length, the time required for *trans*-to-*cis* (140 s) and *cis*-to-*trans* (260 s) isomerization of individual C_3-AMT and C_9-AMT is identical in dichloromethane solution. When a similar experiment was performed using a solution of C_3-NCs and C_9-NCs, it resulted in self-assembled disc-like superstructures. Notably, the *trans*-to-*cis* photoswitching in C_3-NC could reach only 65% even after 460 seconds of irradiation. On the other hand, C_9-NC completed this process within 160 seconds of irradiation. The low photoswitching efficiency of the C_3-NC analog is due to the short and rigid spacer length of C_3-AMT ligands, which are in close proximity to the NC surface, resulting in steric hindrance experienced at the NC–chromophore interface. Importantly, the slow photoswitching in C_3-NCs helps isolate and investigate the intermediates of assembly. Using high-resolution electron microscopy, atomic force microscopy, and 3D reconstruction, we show that the discs are made up of densely packed arrays of NCs. The prolonged illumination of C_9-NCs results in a chain-like assembly due to the dipolar attraction between the previously assembled superstructures. The efficient photoisomerization of chromophores located away from the nanocluster surface has been identified as the key element to speed up the light-induced assembly in chromophore-tethered nanoclusters. Such information will be useful while developing nanoscale photoswitches for electrochemistry, biosensors, and electronic devices.

Received 6th May 2024,
Accepted 3rd July 2024

DOI: 10.1039/d4nr01954g

rsc.li/nanoscale

Introduction

Precision nanoclusters (NCs) offer atomic-scale control over the metal core and exhibit remarkable photophysical and electrochemical properties.[1–10] Even minor modifications to a single metal atom can have a major influence on the behavior and functionality of NCs.[11–16] This characteristic makes NCs ideal building blocks for constructing two-dimensional and three-dimensional self-assembled superstructures with collective and enhanced properties.[17–20] The delicate balance between non-covalent interactions (van der Waals interactions, hydrogen bonding, C–H···π/π···π interactions, electrostatic interactions, aurophilic interactions, amphiphilic interactions, or light-induced dipole–dipole attractions) and thermodynamics controls the generation of self-assembled superstructures, emphasizing the complexity of the assembly process.[21–30] Such assembled materials find applications in device fabrication,[31–34] green catalysis,[35–39] toxin/metal ion screening,[40] gas sensing,[41,42] bioimaging, and therapeutics.[43–47] Among the different non-covalent interactions, light-induced dipolar interaction is promising as it allows reversible assembly by changing the wavelength of light. Studies on the photoswitching properties of azobenzene functionalized gold nanoparticles are well-documented in the literature for over two decades.[48–51] Recently, twenty-five atom

[a]*Smart Materials Lab, Department of Nanoscience and Technology (DNST), University of Calicut, Thenhipalam 673635, Kerala, India. E-mail: shibu@uoc.ac.in*
[b]*Faculty of Engineering and Natural Sciences, Tampere University, P.O. Box 541, FI-33101 Tampere, Finland*

†Electronic supplementary information (ESI) available: Experimental details, ^{1}H, ^{13}C, FT-IR, and LC-MS of molecules; energy-minimized structures and temporal absorption spectra of M3 and M5 molecules; XPS spectra of PET-NC, C_3-NC, and C_9-NC; HR-TEM images and temporal absorption spectra of C_3-NC, and C_9-NC; STEM micrographs and elemental maps of C_3-NC and C_9-NC assemblies; AFM images of C_3-NC and C_9-NC assemblies; TEM images of C_3-NC and C_9-NC self-assembled monomers, dimers, and trimers; TEM images of C_3-NC and C_9-NC assemblies after one year; temporal TEM images of a C_9-NC assembly demonstrate the formation of a disc-like assembly; three-dimensional superstructures are composed of densely packed NCs (MOV). See DOI: **https://doi.org/10.1039/d4nr01954g**

gold (Au_{25}) NCs functionalized with thiolated-spiropyran or -azobenzene ligands demonstrated the feasibility of light-induced reversible self-assembly for hierarchical structure formation across length scales.[29,52,53] These studies have shown that when azobenzene molecules are attached to the surface of NCs, their dipole moments play a significant role in the assembly process. Light irradiation triggers the *trans*-to-*cis* isomerization, resulting in an induced dipole moment. This leads to attractive interactions between neighboring NCs, and forms assembled superstructures. Similar photochemistry has been utilized in systems containing other metal clusters and inorganic nanocages.[54–56] However, the extent of assembly largely depends on the photoswitching efficiency of the chromophores attached to the NC surface. This efficiency is influenced by the chemical structure of the chromophore and its proximity to the NC surface. Thus, NCs functionalized with photoswitchable ligands offer facile control over self-assembly kinetics and structural diversity of self-assembled structures. Here, we show the interplay between the spacer length and photoswitching ability of azobenzene alkyl monothiol (AMT) capped Au NCs. We used AMT-protected NCs (C_3-NCs and C_9-NCs) with two different spacer lengths (C_3-AMT and C_9-AMT). The assembly process of both NCs in dichloromethane (DCM) solution at ambient temperature under 345 nm light was investigated using different spectroscopic studies and microscopic imaging. The C_9-NCs showed quicker self-assembly compared to the C_3 analog due to negligible steric hindrance experienced at the NC–chromophore interface resulting from their safer separation. The fewer nonbonding steric interactions allow more favorable orientation and arrangement to the surface chromophores, forming self-assembled superstructures *via* attractive dipoles. Prolonged illumination of C_9-NCs showed a chain-like assembly due to the dipolar attraction between nearby superstructures. These findings highlight the importance of rational design and control over the spatial arrangement of chromophores in precision NCs. By carefully tuning the spacer length and considering the steric effects, it becomes feasible to optimize the self-assembly process and achieve desired supramolecular structures with enhanced photophysical and electrochemical properties.

Results and discussion

To investigate the role of chromophore–spacer length in the light-induced assembly of NCs, we first covalently linked the azobenzene core with the C_3-carbon chain (short; C_3-AMT) and C_9-carbon chain (long; C_9-AMT) thiols (Fig. 1a). The synthesis and characterization of the ligands are presented in the ESI (Fig. S1–S15†). The time-dependent absorption spectra obtained from C_3-AMT and C_9-AMT dispersed in DCM and irradiated separately using UV light (345 nm) are shown in Fig. 1b and c, respectively. The systematic decrease in optical density (OD) at 345 nm and simultaneous gradual increase in OD around 435 nm indicate the *trans*-to-*cis* isomerization of azobenzene moieties. The absorption spectra of C_3-AMT and C_9-AMT show the *cis*-to-*trans* isomerization when irradiated at 435 nm (Fig. S16a and b†). The energy-minimized structures of *cis*/*trans* geometrical isomers of C_3 and C_9-AMT obtained through density functional theory (DFT) are illustrated in the inset of Fig. 1b and Fig. S17,† respectively. From the combined plot of OD@345 nm *vs.* irradiation time of C_3-AMT and C_9-AMT recorded under 345 nm and 435 nm light, it is evident that the time required for *trans*-to-*cis* (~140 s) and *cis*-to-*trans* (~260 s) isomerization in AMT is nearly identical, irrespective of the spacer length (inset in Fig. 1c). However, the *cis*-to-*trans* conversion was not complete due to the overlap of the n–π* transition of *cis* and *trans* isomers.[57]

To evaluate the role of chromophore–spacer length in the light-induced assembly of NCs, photoswitchable gold NCs with two different spacer lengths (C_3-NC and C_9-NC) were synthesized and purified using the procedure reported for $[Au_{144}(PET)_{60}]$ NCs (abbreviated as PET-NC; Fig. 1a, see the ESI† for details; here PET represents 2-phenylethanethiol). The optical absorption features of C_3 and C_9 NCs were compared with those of the PET analog (PET-NC; Fig. 1d). The presence of two weak humps at *ca.* 520 nm and 700 nm, similar to that of PET-NC, and an overlapping absorption maximum at 345 nm equivalent to the optical absorption characteristics of AMT confirms the formation of C_3 and C_9 NCs. Since electrospray ionization mass spectrometry (ESI-MS) and matrix-assisted laser desorption ionization (MALDI) mass spectrometry trials were not successful, we compared the X-ray photoelectron spectra (XPS) of C_3-NC and C_9-NC with that of PET-NC. The well-matching binding energy (BE) values of gold 4f electron orbitals in C_3-NC and C_9-NC compared to the reported values of PET-NC (inset in Fig. 1d) suggest a similar metal core for all the three NCs (C_3-NC, C_9-NC, and PET-NC). A small shift in the BE of the NCs is presumably due to the difference in the electron densities of the organic counterparts. The BE values of C 1s, N 1s, O 1s, and S 2p levels of all three NCs are shown in Fig. S18a–d.† The core size of C_3-NC and C_9-NC was examined using TEM (transmission electron microscopy) analysis. TEM images of C_3- and C_9-NCs (inset in Fig. 2a and Fig. S19,† respectively) show nearly uniform size distributions (1.9 ± 0.14 nm and 1.87 ± 0.12 nm). The core sizes of C_3- and C_9-NCs are in agreement with that of PET-NC.[58] Next, we evaluated the photoisomerization efficiency of C_3 and C_9 NC solutions in DCM under two different wavelengths of light. The absorption spectra of C_3 and C_9 NCs illuminated under 345 nm are shown in Fig. 2a and b, respectively. The time-dependent absorption spectra of C_3 and C_9 NCs recorded separately during the reverse (*cis*-to-*trans*) photoswitching (435 nm) are shown in Fig. S20a and b.† The combined plots of OD@345 nm *vs.* irradiation time recorded during the photoisomerization (*trans*-to-*cis* and *cis*-to-*trans*) of C_3 and C_9 NCs are shown in the inset of Fig. 2b. Notably, the time required for *trans*-to-*cis* photoswitching in C_3 and C_9 NCs (same concentration) under a similar intensity of light (0.2 mW cm^{-2}) was found to be different. More precisely, the *trans*-to-*cis* photoswitching in C_3-NC could reach only 65%

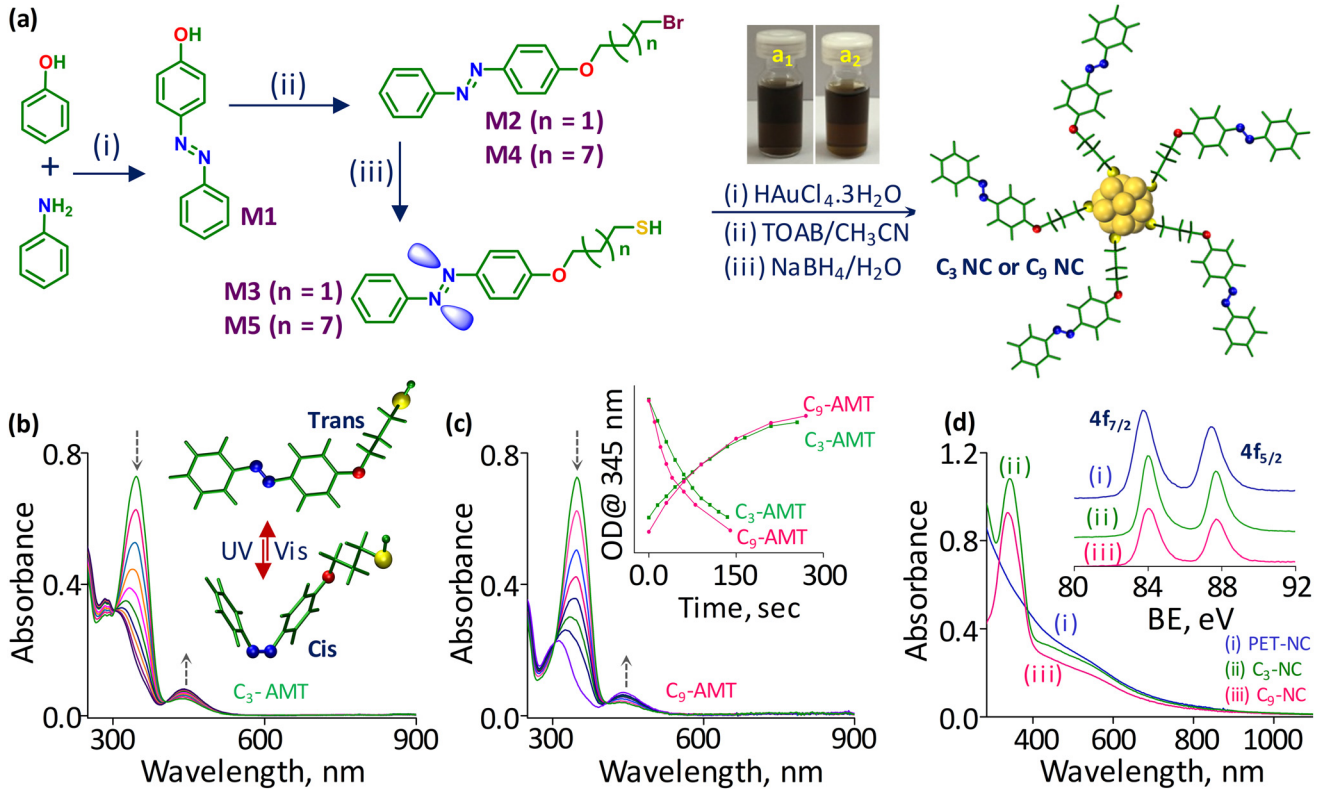

Fig. 1 (a) Synthesis schemes of C_3-AMT and C_9-AMT (M1–M5), C_3-NC, and C_9-NC; (i) conc. HCl, $NaNO_2$, 0 °C, (ii) 1,3-dibromopropane or 1,9-dibromononane, K_2CO_3, KI, acetone, 80 °C, and (iii) HMDST and TBAF, distilled THF, −10 °C. The photographs of C_3 and C_9 NC solutions are shown in a_1 and a_2. (b and c) The temporal optical absorption spectra of (b) C_3-AMT and (c) C_9-AMT under 345 nm illumination. Energy-minimized structures of *trans* and *cis* isomers of C_3-AMT are shown in the inset of b. Combined plots of OD (*ca.* 345 nm) *vs.* illumination time recorded from C_3-AMT and C_9-AMT under 345 nm and 435 nm are given in the inset of c. (d) UV-Vis absorption spectra of (i) PET-NC, (ii) C_3-NC and (iii) C_9-NC recorded in DCM. The XPS spectra (Au 4f levels) of all three NCs are shown in the inset of d.

even after 460 seconds of illumination. Beyond this point, there was no change in their absorbance.

On the other hand, C_9-NC completed the isomerization process within 160 seconds of illumination. Importantly, the *trans*-to-*cis* isomerization in C_9-NC is comparable to that of free AMT molecules (inset in Fig. 1c; 140 s), while the isomerization is three times slower in the case of C_3-NCs. This suggests the effect of chromophore proximity on photoswitching. In C_9-NCs, the chromophore is located far from the metal surface. Furthermore, the spacer is flexible, allowing less steric crowding. However, in C_3-NCs the short spacer is rigid, and the chromophore is in close proximity to the NC surface, resulting in steric crowding of surface ligands. Therefore, the steric hindrance experienced at the NC–chromophore interface finally restricts the photoswitching process. To understand the role of chromophore–spacer length in the self-assembly of NCs and investigate the resulting superstructures, we used TEM imaging. For this, ~100 μM solutions of C_3 and C_9 NCs prepared in DCM separately were irradiated at 345 nm for 90 min in a dark room. Constant stirring of the NC solutions in a temperature-controlled bath helped to reduce thermal aggregation. The TEM images of the illuminated C_3 and C_9 NCs are shown in Fig. 2c and d, respectively. Though C_3 and C_9 NCs underwent light-induced self-assembly and formed disc-like superstructures, there are some morphological differences in the superstructures formed from both NCs. TEM images of individual superstructures from C_3 and C_9 NCs are shown in Fig. 2e and f, respectively. The C_3-NCs are self-assembled into disc-like superstructures with a crystallized array of NCs encapsulated in each superstructure (Fig. 2g). This is presumably due to the slow assembly and the rigid nature of the ligands, which promote a well-ordered array of NCs. Furthermore, an incomplete and slow isomerization may also affect the assembly kinetics, resulting in heterogeneous structures. On the other hand, the C_9-NC superstructure (Fig. 2h) showed a nearly uniform assembly of densely packed structures. From the above spectroscopic and microscopic studies, it is obvious that the timescale of light-induced self-assembly largely depends on the suitable distance between the chromophores and NCs. The uniform assembly in C_9-NC compared to that in the C_3 analog is attributed to the negligible steric hindrance experienced at the NC–chromophore interface. The schematic shows the distance-dependent self-assembly in C_3 and C_9 NCs and the possible mechanism for their slow and quick assembly is shown in Fig. 2i. The structural details of self-assembled superstructures were further explored using dark-field scan-

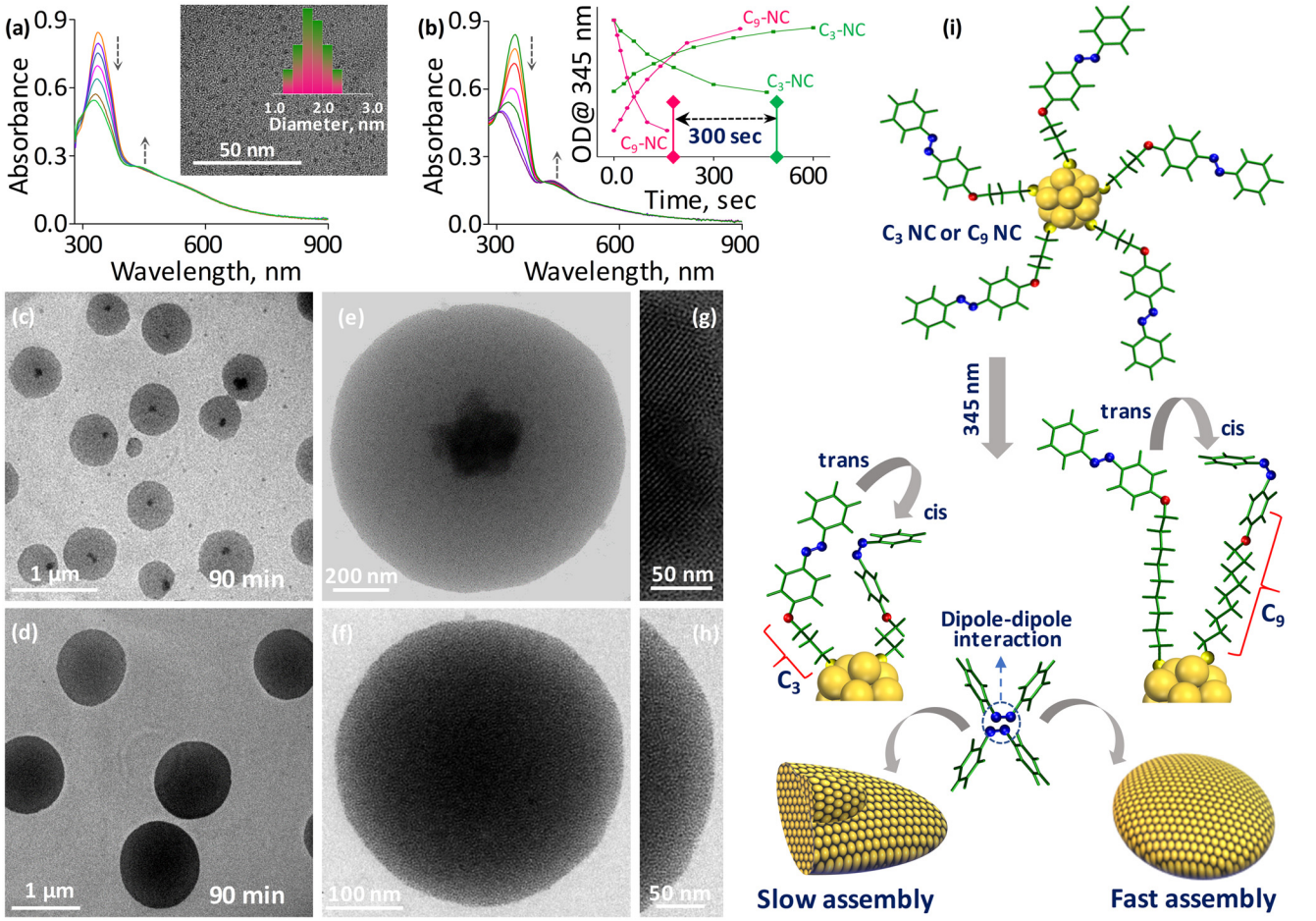

Fig. 2 (a and b) Temporal optical absorption spectra recorded from (a) C_3-NC and (b) C_9-NC under 345 nm illumination. The TEM micrograph of C_3-NC is shown in the inset of a. The combined plots of OD (*ca.* 345 nm) *vs.* irradiation time, under 345 nm and 435 nm light recorded from C_3-NC and C_9-NC are shown in the inset of b. (c and d) Large area TEM images captured from (c) C_3-NC and (d) C_9-NC assembly after 90 min of illumination under 345 nm light. (e and f) Magnified and tightly focused TEM micrographs of a single superstructure derived from (e) C_3-NC and (f) C_9-NC. (g and h) An enlarged image captured from (g) the center dark spot of C_3-NC and (h) the edge of C_9-NC assemblies. (i) The schematic shows the distance-dependent self-assembly in C_3-NC and C_9-NC and the possible mechanism for their slow and quick assembly.

ning transmission electron microscopy (STEM) imaging and elemental mapping. The STEM images of C_3- and C_9-NC assemblies are shown in Fig. S21a and b,† respectively. High contrast in the STEM image of the C_3-NC assembly at the center shows the existence of crystallized aggregates encapsulated within the disc-like structures (Fig. S21c†). The STEM micrograph of the C_9-NC assembly shows uniform contrast all over the surface (Fig. S21d†). The chemical composition assessment of both self-assembled superstructures using energy-dispersive X-ray analysis (EDS) verifies the existence of gold, sulfur, nitrogen, oxygen, and carbon. The gold (yellow) and sulfur (green) mappings of single superstructures derived from C_3- and C_9-NCs are shown in Fig. S21e–h.† The large area STEM images, elemental maps (gold, sulfur, and nitrogen), and EDS spectra recorded from C_3- and C_9-NC assemblies are shown in the ESI (Fig. S22†).

Furthermore, field emission scanning electron microscopy (FESEM) and atomic force microscopy (AFM) images were utilized to investigate the structural details of assembled superstructures. Fig. 3a and b show the FESEM micrographs captured from C_3- and C_9-NC assemblies. The disc-like superstructures with a few layers of subsequent assemblies on the top surface are seen in the case of the C_3-NC assembly. The C_9-NC assembly shows densely packed disc-like superstructures similar to those observed in the TEM image shown in Fig. 2d. The morphology of the assembled superstructures was further examined using AFM imaging. Fig. S23a and b† show the large-area AFM images captured from C_3- and C_9-NC assemblies, in which the subsequent assemblies are visible in the case of C_3-NC. The AFM images of single superstructures derived from C_3- and C_9-NCs are shown in Fig. S24.† The AFM data are consistent with TEM, STEM, and FESEM results. The high-resolution AFM images captured from a single superstructure derived from C_3-NC (Fig. 3c–g) show the periodic assembly of NCs. The zig-zag patterns represent the NC directions in the assembly (Fig. 3d and e).

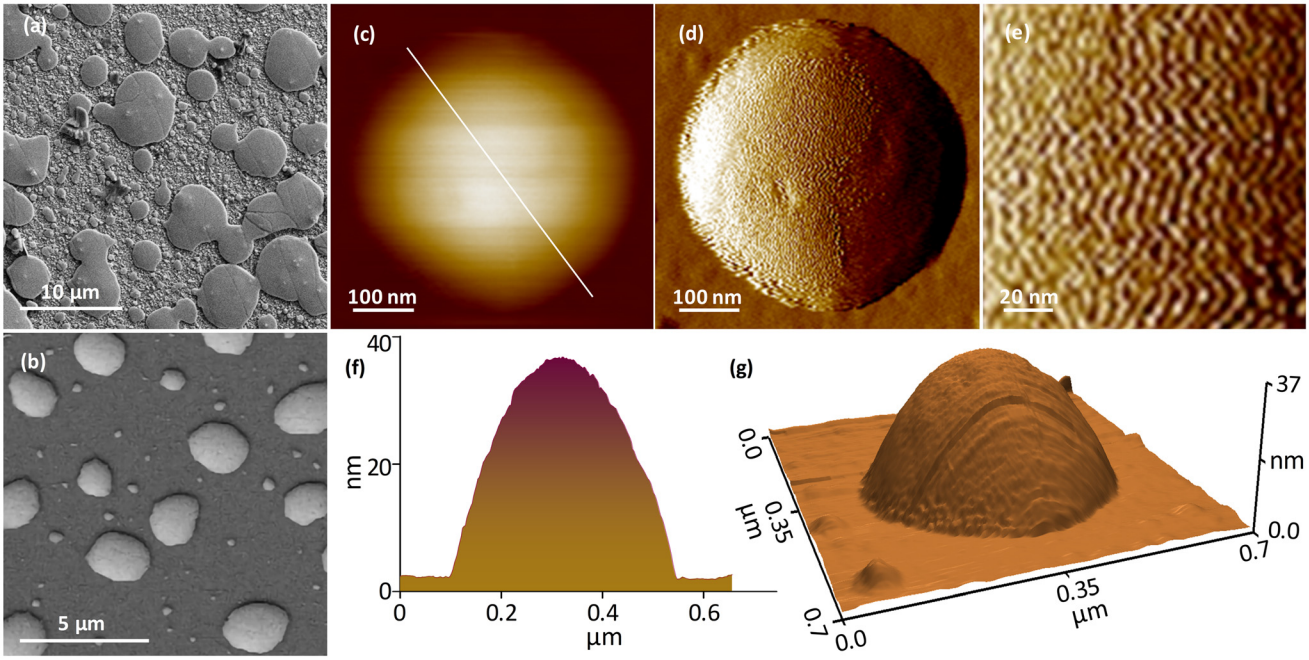

Fig. 3 (a and b) FESEM images of (a) C_3-NC and (b) C_9-NC assemblies. (c and d) High-resolution tapping mode AFM (c: topography and d: amplitude) images of the single superstructure derived from C_3-NC. (e) A zoomed and focused AFM image captured from the top surface of the C_3-NC assembly showing the NC direction in the assembly. (f and g) The height profile and three-dimensional (3D) AFM image of the same assembly.

To further gain insights into the 3D internal structures of self-assembled structures, we used electron tomography (ET).[59] Details are provided in the ESI.† Accordingly, the 2D projections were collected over a range of ±70° with an increment angle of 2° (Fig. S25†). The corresponding TEM images (Fig. 4a and b) and the 3D reconstruction images of C_3- and C_9-NC assemblies (Fig. 4c–g, Videos S1 and S2†) revealed the disc-like morphology of the superstructures. The cross-sectional view suggests that the superstructures are composed of densely packed NC networks. However, there is a significant difference in the overall disc thickness. As observed in 2D projections, the C_3 NCs contain crystalline aggregates within the discs that protrude outside the discs (Fig. 4c, e, and f). On the other hand, a uniform array of NCs was observed in the case of C_9 NC-based assemblies (Fig. 4d and g). It is important to note that deformed shapes and flattening are commonly observed in such assemblies due to solvent evaporation and drying artifacts during specimen preparation. However, we observed a clear difference in the 3D reconstructed structures obtained from C_3 NCs and C_9 NCs. Superstructures obtained from C_3 NCs display uniform thickness across the particle. This suggests that the superstructures are disc-like assemblies. On the other hand, in the case of C_9 NCs, the deformation and flattening of the structure are evident due to the non-uniform thickness between the center and the periphery.

NCs were also assembled into dimer and trimer superstructures during the light-induced self-assembly. However, the percentage of dimers and trimers formed was significantly lower compared to that of the monomer assembly. The early stages of monomer, dimer, and trimer assemblies derived from C_9-NCs are shown in Fig. S26,† in which the dimer and the trimer show well-connected interfaces with periodic assembly. Eventually, they transformed into densely packed superstructures with constant illumination under 345 nm light (Fig. S27†). The early stages of dimer and trimer assemblies fabricated from C_3-NCs with a few layers of incomplete assemblies similar to the monomer are shown in Fig. S28.† Subsequently, we investigated the long-term stability of the assembled superstructures using TEM imaging of the same grid stored at low temperature. Notably, the morphology of the assembly was intact even after one year (Fig. S29†). To understand the formation of disc-like assemblies, TEM imaging was performed on samples prepared using a solution of C_9-NC in DCM under 345 nm illumination at different time intervals. The TEM images revealed the formation of disc-like superstructures that evolved from the short circular assembly (Fig. S30†).

We finally investigated the impact of prolonged illumination on the structural transformation of the assembled superstructures. For this, a solution of C_9-NC in DCM was UV irradiated at 345 nm for 5 h. The sustained illumination resulted in the solidification of NCs due to the formation of bulky superstructures. To understand the structural rearrangements, the solid material was further examined by redissolving it in DCM. The FESEM image (Fig. 5b) shows a chain-like assembly formed by fusing the individual superstructures due to dipole–dipole interactions between them. A similar chain-like framework seen using the dark-field scattering microscope (Fig. 5c) is in good agreement with the FESEM data. The TEM micrographs captured from the surface and edge of the chain-like

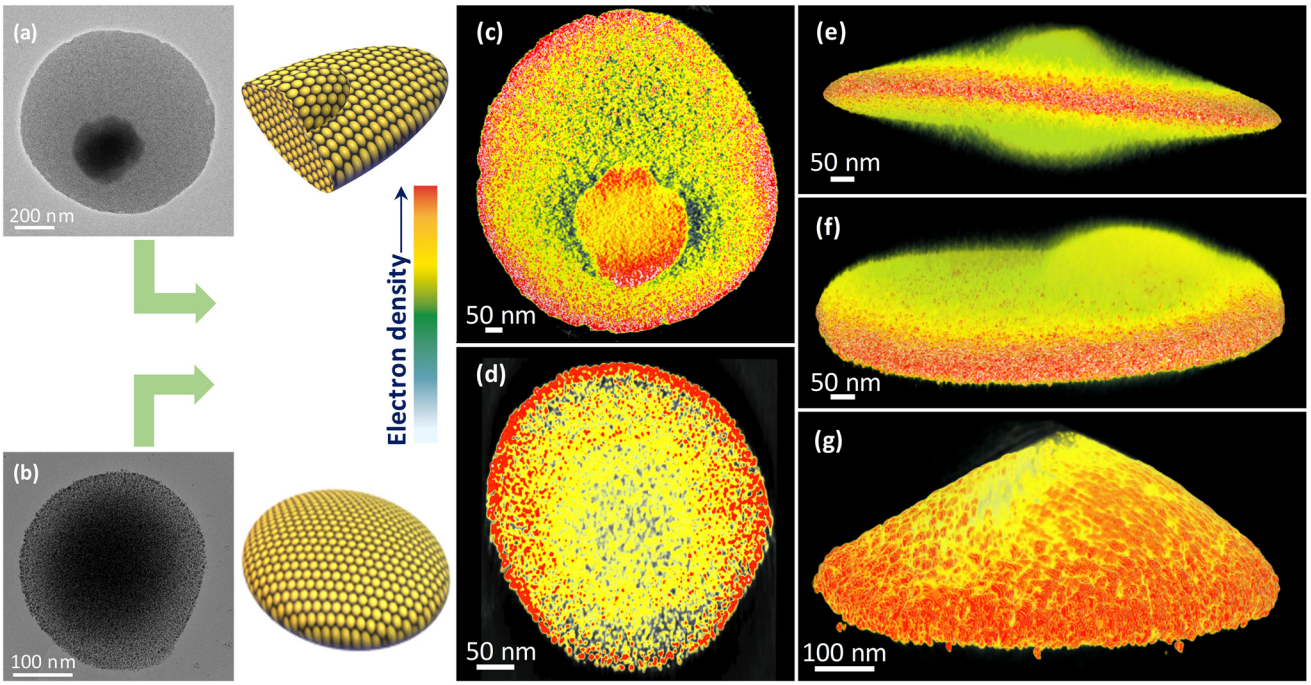

Fig. 4 (a and b) TEM images and (c and d) corresponding cross-sectional views from the ET reconstructed images of (a and c) C_3-NC and (b and d) C_9-NC superstructures. (e–g) The 3D-reconstructed tomograms of (e and f) C_3-NC and (g) C_9-NC superstructures in different orientations.

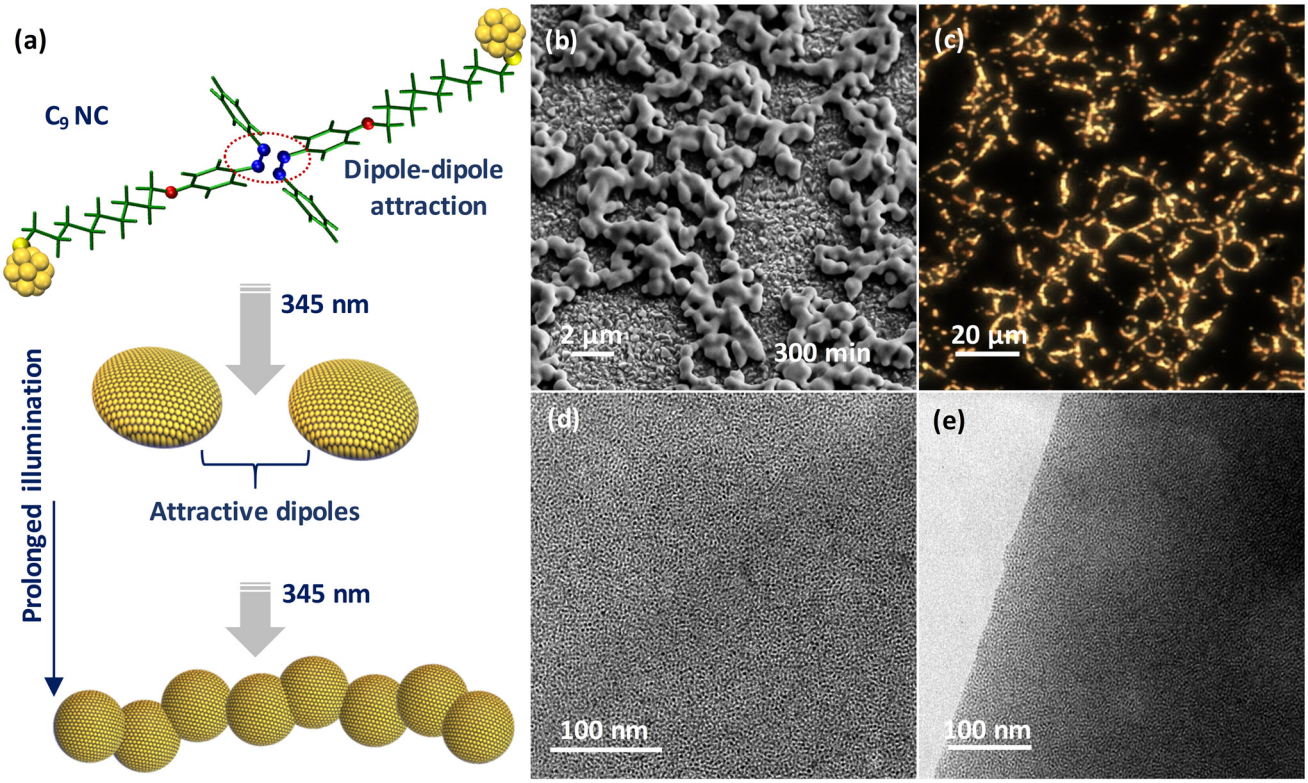

Fig. 5 (a) The schematic depicts the formation of a chain-like assembly. (b) FESEM and (c) dark-field scattering images of the chain-like assembly. (d and e) TEM micrographs from the surface and edge of the chain-like assembly.

structures (Fig. 5d and e) showed a highly ordered multilayer assembly throughout. A scheme for the formation of a chain-like assembly is shown in Fig. 5a, in which the individual NCs initially self-assembled into disc-like superstructures and then into chain-like assemblies due to the extended dipolar interactions between them during the course of illumination. The above-demonstrated idea will be useful in fulfilling industrial needs, especially in the development of molecular photoswitches.

Conclusions

The reversible self-assembly of NCs using external stimuli such as light, heat, and magnetic fields is a tremendously evolving research area. In the recent past, light has been identified as an efficient probe to demonstrate the supramolecular self-assembly of chromophore-tethered NCs. However, the magnitude of assembly in chromophore-tethered NCs largely depends on their photoswitching efficiency. We have successfully demonstrated this concept by introducing two photoswitchable NCs fabricated using thiolated-azobenzene molecules with different spacer lengths. The core and molecular information of both NCs were meticulously explored using various spectroscopic and microscopic techniques. Photoactivation of both NC solutions at ambient temperature using 345 nm light resulted in the formation of self-assembled superstructures. FESEM, AFM, TEM, ET reconstruction, STEM, and dark field scattering microscopic studies showed the presence of densely packed NCs in self-assembled superstructures. By introducing the idea of distance dependency, we successfully demonstrated the prompt self-assembly in NCs. This was evident from the fast assembly observed in C_9-NCs due to their improved photoswitching efficiency resulting from the negligible steric hindrance experienced at the NC–chromophore interface. Such molecular control over the self-assembly of NCs by placing the chromophores suitably away from the nanosurface is useful for developing next-generation switchable sensors, especially in biological, electrochemical, and electronic devices.

Author contributions

The project was designed and supervised by E. S. S. The chromophores and nanoclusters were synthesized by J. V. R. All the experiments were performed by E. S. S. and J. V. R. The electron tomography data acquisition and reconstruction were performed by N. The manuscript was written through the contributions of all authors. All authors have given approval to the final version of the manuscript.

Data availability

The data supporting this article have been included as part of the ESI.†

Conflicts of interest

There are no conflicts to declare.

Acknowledgements

E. S. S. thanks the Science and Engineering Research Board (SERB) for the Ramanujan Fellowship (SB/S2/RJN-005/2017) and Start-up Research grant (SRG/2022/586). E. S. S. thanks the Department of Science and Technology (DST), India, for the Promotion of University Research and Scientific Excellence grant (PURSE; SR/PURSE/2023/191). E. S. S. thanks the University of Calicut for the seed money grant. The authors thank the DST Unit of Nanoscience (DST-UNS) and Thematic Unit of Excellence (TUE), IIT Madras, for HRTEM measurements and DFT calculations. The authors thank the Central Instrumentation Facility (CIF), CSIR-CECRI, for the instrumentation support. J. V. R. thanks the SERB for supporting the research fellowship. The authors thank the Academy of Finland for project funding (No. 352900) and the Photonic Research and Innovation (PREIN) flagship. This work made use of the Tampere Microscopy Centre facilities at Tampere University, Finland.

References

1 R. L. Whetten, J. T. Khoury, M. M. Alvarez, S. Murthy, I. Vezmar, Z. L. Wang, P. W. Stephens, C. L. Cleveland, W. D. Luedtke and U. Landman, *Adv. Mater.*, 1996, **8**, 428–433.
2 G. Schmid, M. Bäumle, M. Geerkens, I. Heim, C. Osemann and T. Sawitowski, *Chem. Soc. Rev.*, 1999, **28**, 179–185.
3 Y. Negishi, K. Nobusada and T. Tsukuda, *J. Am. Chem. Soc.*, 2005, **127**, 5261–5270.
4 H. Häkkinen, *Chem. Soc. Rev.*, 2008, **37**, 1847–1859.
5 R. Jin, C. Zeng, M. Zhou and Y. Chen, *Chem. Rev.*, 2016, **116**, 10346–10413.
6 W. Kurashige, Y. Niihori, S. Sharma and Y. Negishi, *Coord. Chem. Rev.*, 2016, **320–321**, 238–250.
7 I. Chakraborty and T. Pradeep, *Chem. Rev.*, 2017, **117**, 8208–8271.
8 K. Kwak and D. Lee, *Acc. Chem. Res.*, 2019, **52**, 12–22.
9 M. Hesari and Z. Ding, *Acc. Chem. Res.*, 2017, **50**, 218–230.
10 Y.-M. Su, Z. Wang, C.-H. Tung, D. Sun and S. Schein, *J. Am. Chem. Soc.*, 2021, **143**, 13235–13244.
11 X. Kang and M. Zhu, *Chem. Soc. Rev.*, 2019, **48**, 2422–2457.
12 X. Kang, S. Chen, S. Jin, Y. Song, Y. Xu, H. Yu and H. Sheng, *ChemElectroChem*, 2016, **25**, 1–6.
13 W. Fei, S. Antonello, T. Dainese, A. Dolmella, M. Lahtinen, K. Rissanen, A. Venzo and F. Maran, *J. Am. Chem. Soc.*, 2019, **141**, 16033–16045.
14 W. Kurashige, R. Hayashi, K. Wakamatsu, Y. Kataoka, S. Hossain, A. Iwase, A. Kudo, S. Yamazoe and Y. Negishi, *ACS Appl. Energy Mater.*, 2019, **2**, 4175–4187.

15 S. Wang, Q. Li, X. Kang and M. Zhu, *Acc. Chem. Res.*, 2018, **51**, 2784–2792.
16 A. Ghosh, O. F. Mohammed and O. M. Bakr, *Acc. Chem. Res.*, 2018, **51**, 3094–3103.
17 P. Chakraborty, A. Nag, A. Chakraborty and T. Pradeep, *Acc. Chem. Res.*, 2019, **52**, 2–11.
18 Z. Wu, Q. Yao, S. Zang and J. Xie, *ACS Mater. Lett.*, 2019, **1**, 237–248.
19 J. V. Rival, P. Mymoona, K. M. Lakshmi, Nonappa, T. Pradeep and E. S. Shibu, *Small*, 2021, **17**, 2005718.
20 Nonappa, *Chem. Commun.*, 2023, **59**, 13800–13819.
21 Z. Wu, J. Liu, Y. Li, Z. Cheng, T. Li, H. Zhang, Z. Lu and B. Yang, *ACS Nano*, 2015, **9**, 6315–6323.
22 Nonappa, T. Lahtinen, J. S. Haataja, T.-R. Tero, H. Häkkinen and O. Ikkala, *Angew. Chem., Int. Ed.*, 2016, **55**, 16035–16038.
23 B. Yoon, W. D. Luedtke, R. N. Barnett, J. Gao, A. Desireddy, B. E. Conn, T. Bigioni and U. Landman, *Nat. Mater.*, 2014, **13**, 807–811.
24 L. Shi, L. Zhu, J. Guo, L. Zhang, Y. Shi, Y. Zhang, K. Hou, Y. Zheng, Y. Zhu, J. Lv, S. Liu and Z. Tang, *Angew. Chem., Int. Ed.*, 2017, **56**, 15397–15401.
25 T. Higaki, C. Liu, M. Zhou, T.-Y. Luo, N. L. Rosi and R. Jin, *J. Am. Chem. Soc.*, 2017, **139**, 9994–10001.
26 L. He, Z. Gan, N. Xia, L. Liao and Z. Wu, *Angew. Chem., Int. Ed.*, 2019, **58**, 9897–9901.
27 Z. Wu, Y. Du, J. Liu, Q. Yao, T. Chen, Y. Cao, H. Zhang and J. Xie, *Angew. Chem., Int. Ed.*, 2019, **58**, 8139–8144.
28 Q. Yao, X. Yuan, Y. Yu, Y. Yu, J. Xie and J. Y. Lee, *J. Am. Chem. Soc.*, 2015, **137**, 2128–2136.
29 J. V. Rival, Nonappa and E. S. Shibu, *ACS Appl. Mater. Interfaces*, 2020, **12**, 14569–14577.
30 P.-P. Sun, B.-L. Han, H.-G. Li, C.-K. Zhang, X. Xin, J.-M. Dou, Z.-Y. Gao and D. Sun, *Angew. Chem., Int. Ed.*, 2022, **61**, e202200180.
31 Z. Wu, J. Liu, Y. Gao, H. Liu, T. Li, H. Zou, Z. Wang, K. Zhang, Y. Wang, H. Zhang and B. Yang, *J. Am. Chem. Soc.*, 2015, **137**, 12906–12913.
32 Y. Liu, D. Yao and H. Zhang, *ACS Appl. Mater. Interfaces*, 2018, **10**, 12071–12080.
33 H.-Y. Huang, K.-B. Cai, M. J. Talite, W.-C. Chou, P.-W. Chen and C.-T. Yuan, *Sci. Rep.*, 2019, **9**, 4053.
34 P. Sun, Z. Wang, Y. Bi, D. Sun, T. Zhao, F. Zhao, W. Wang and X. Xin, *ACS Appl. Nano Mater.*, 2020, **3**, 2038–2046.
35 Z. Wu, Y. Li, J. Liu, Z. Lu, H. Zhang and B. Yang, *Angew. Chem., Int. Ed.*, 2014, **53**, 12196–12200.
36 Z. Wu, H. Zou, T. Li, Z. Cheng, H. Liu, Y. Liu, H. Zhang and B. Yang, *Chem. Commun.*, 2017, **53**, 416–419.
37 Y. Zhu, X. Qiu, S. Zhao, J. Guo, X. Zhang, W. Zhao, Y. Shi and Z. Tang, *Nano Res.*, 2020, **13**, 1928–1932.
38 M. Cao, R. Pang, Q.-Y. Wang, Z. Han, Z.-Y. Wang, X.-Y. Dong, S.-F. Li, S.-Q. Zang and T. C. W. Mak, *J. Am. Chem. Soc.*, 2019, **141**, 14505–14509.
39 C. Deng, C. Sun, Z. Wang, Y. Tao, Y. Chen, J. Lin, G. Luo, B. Lin, D. Sun and L. Zheng, *Angew. Chem., Int. Ed.*, 2020, **59**, 12659–12663.
40 J. Benavides, I. Quijada-Garrido and O. García, *Nanoscale*, 2020, **12**, 944–955.
41 R. Huang, Y. Wei, X. Dong, X. Wu, C. Du, S.-Q. Zang and T. C. W. Mak, *Nat. Chem.*, 2017, **9**, 689–697.
42 X.-Y. Dong, Y. Si, J.-S. Yang, C. Zhang, Z. Han, P. Luo, Z.-Y. Wang, S.-Q. Zang and T. C. W. Mak, *Nat. Commun.*, 2020, **11**, 3678.
43 A. Yahia-Ammar, D. Sierra, F. Mérola, N. Hildebrandt and X. Le Guével, *ACS Nano*, 2016, **10**, 2591–2599.
44 M. Hembury, N. Beztsinna, H. Asadi, J. B. van den Dikkenberg, J. D. Meeldijk, W. E. Hennink and T. Vermonden, *Biomacromolecules*, 2018, **19**, 2841–2848.
45 L. Yang, H. Wang, D. Li, L. Li, X. Lou and H. Liu, *Chem. Mater.*, 2018, **30**, 5507–5515.
46 M. Wang, Y. Chen, W. Cai, H. Feng, T. Du, W. Liu, H. Jiang, A. Pasquarelli, Y. Weizmann and X. Wang, *Proc. Natl. Acad. Sci. U. S. A.*, 2020, **117**, 308–316.
47 S. Biswas, A. K. Das, A. Nath, S. Paul, M. S. Singh and S. Mandal, *Nanoscale*, 2021, **13**, 17325–17330.
48 J. Zhang, J. K. Whitesell and M. A. Fox, *Chem. Mater.*, 2001, **13**, 2323–2331.
49 S. Bonacchi, A. Cantelli, G. Battistelli, G. Guidetti, M. Calvaresi, J. Manzi, L. Gabrielli, F. Ramadori, A. Gambarin, F. Mancin and M. Montalti, *Angew. Chem., Int. Ed.*, 2016, **55**, 11064–11068.
50 A. Köhntopp, A. Dabrowski, M. Malicki and F. Temps, *Chem. Commun.*, 2014, **50**, 10105.
51 R. Klajn, J. F. Stoddart and B. A. Grzybowski, *Chem. Soc. Rev.*, 2010, **39**, 2203.
52 Y. Negishi, U. Kamimura, M. Ide and M. Hirayama, *Nanoscale*, 2012, **4**, 4263–4268.
53 T. Udayabhaskararao, P. K. Kundu, J. Ahrens and R. Klajn, *ChemPhysChem*, 2016, **17**, 1805–1809.
54 L. Ai, Y. Li, Z. Wu, J. Liu, Y. Gao, Y. Liu, Z. Lu, H. Zhang and B. Yang, *J. Phys. Chem. C*, 2016, **120**, 24427–24436.
55 Y. Deng, Y. Wu, Z. Li, Z. Jagličić, R. K. Gupta, C. Tung and D. Sun, *Chin. J. Chem.*, 2023, **41**, 1667–1672.
56 K. Sheng, Y.-N. Liu, R. K. Gupta, M. Kurmoo and D. Sun, *Sci. China: Chem.*, 2021, **64**, 419–425.
57 Z. Wu, R. Xue, M. Xie, X. Wang, Z. Liu, M. Drechsler, J. Huang and Y. Yan, *J. Phys. Chem. Lett.*, 2018, **9**, 163–169.
58 N. Yan, N. Xia, L. Liao, M. Zhu, F. Jin, R. Jin and Z. Wu, *Sci. Adv.*, 2018, **144**, 1–8.
59 Nonappa, *ACS Mater. Au*, 2024, **4**, 238–257.